Energy & Environmental Science

Accepted Manuscript

ROYAL SOCIETY OF CHEMISTRY

www.rsc.org/ees

The photoelectrochemical performance of semiconducting photocatalyst for solar light fuel is related to solar light absorption, charge separation, charge transfer, and charge mobility etc. Such considerations are attributed to the 3-dimensional atomic arrangement on the surface of photocatalyst like coordination bonds between atoms and presence/absence of dangling bond. Tremendous efforts on facet engineering have been approached to various metal and metal oxide microcrystals. Even that some of the theoretical calculation and prediction on the surface energy of crystal facet have been reported, there is lack of study related to proper comparison among thin films with different crystal facets because of difficulty to fabricate thin films with exclusive one axis orientation and block or minimize the other facet exposure. We have suggested the fabrication of exclusively selected one crystal facet exposed metal oxide thin film by three steps, synthesis of microcrystals, monolayered microcrystal and second hydrothermal reaction.

Energy & Environmental Science

ARTICLE

Selectively Exposed Crystal Facet-Engineered TiO_2 Thin Film Photoanode for the Higher Performance of Photoelectrochemical Water Splitting Reaction

Received 00th January 20xx,
Accepted 00th January 20xx

DOI: 10.1039/x0xx00000x

www.rsc.org/

Chang Woo Kim,[a†] So Jin Yeob,[a†] Hui-Ming Cheng[b] and Young Soo Kang[a,*]

In the present study, selectively exposed (101)-crystal facet engineered TiO_2 photoanode is investigated for the higher efficiency of hydrogen evolution reaction. Till date, even the photoelectrochemical performance (PEC) depending on the exposed crystal facet have been calculated and demonstrated in the semiconducting microcrystals, selectively exposed crystal facet of photocatalyst thin films has not been reported yet. Herein, we demonstrate TiO_2 thin film photoanode with 100%-exclusively exposed crystal facet and suggest the methodology for metal oxide thin film photoanode with selectively exposed crystal facet. Selectively exposed crystal facet-manipulated metal oxide thin film photoanode is fabricated over the pre-synthesized microcrystals through a three-step strategy: 1) hydrothermal synthesis of microcrystals, 2) positioning of microcrystals via polymer-induced manual assembly, and 3) fabrication of selectively exposed crystal facet of TiO_2 thin film through secondary growth hydrothermal reaction. Based on the synthesis of representative TiO_2 microcrystals with dominantly exposed (101), (100) and (001) crystal facet, selectively exposed crystal faceted TiO_2 thin film photoanode is comparatively investigated for practical PEC performance. The photocurrent density of selectively exposed (101) crystal faceted TiO_2 thin film photoanode is determined as 0.13 mA cm^{-2} and produce 18% of incident photon-to-current conversion efficiency at 0.65 V Ag/AgCl potential under AM 1.5 G illumination. Its photoelectrochemical hydrogen production reached to 0.07 mmol cm^{-2} for 12 hrs, which is higher than those of (100) and (001) faceted photoelectrode.

Introduction

As an alternative energy to fossil fuels, a solar energy is the most environmental-friendly and promising energy resource.[1-4] From an unlimited solar energy, artificial photosynthesis process has attracted significant attention for the solar fuel production such as hydrogen and C1 fuels. As called artificial photosynthesis process, photoelectrochemical (PEC) process is the suitable integrated energy conversion system for solar fuel production through water photoelectrolysis.[5,6] Such recent development have been devoted to solar light absorption efficiency, charge separation efficiency and surface charge transfer efficiency for integrated solar energy conversion.[7] Especially, strategy for PEC enhancement has been focused on manipulation of photo-reactive exposed crystal faceted photocatalysts since systematic demonstration of surface energy-dependent photocatalytic PEC performance by H-M. Cheng group and C. Lee group.[3,8] They reported the dramatic impact of PEC performance in anatase TiO_2 microcrystal with dominantly exposed (001) facet. Furthermore, {001}, {010}, and {101}-dominantly faceted TiO_2 microcrystal have been manipulated with F^- ion.[9] As motivated with crystal facet-dependent properties of photocatalysts, PEC performance of metal oxide microcrystals of photocatalysts such as facet-selective ZnO nanorod,[10,11] {002}, {200} and {020} facets engineered WO_3 quasi-cubic crystal,[12] polyhedral Cu_2O microcrystal,[13] $BiVO_4$ microcrystals with dominant (040) facet[14] and BiOCl nanosheet with {001} facet[15,16] have been reported recently and suggested for the higher efficiency of water splitting reaction. The atomic arrangement at the crystal surface of selected crystal facet of photocatalysts provides specific photo-activity and reactive site. Such atomic arrangement at the surface leads to the specifically exposed crystal facet to show the enhancement of PEC performance.

Even surface energy calculated from atomic arrangement would be effective for enhanced PEC performance, its enhancement has been demonstrated by photocatalysts with selectively exposed dominant crystal facet.[17,18] Interestingly it would be controversial that its surface energy calculations depending on the selectively exposed crystal facet of photocatalyst microcrystal did not match with the PEC performance of the microcrystals.[9,19] Especially, to better

[a] Korea Center for Artificial Photosynthesis and Department of Chemistry, Sogang University, Seoul 121-742, Republic of Korea.
[b] Shenyang National Laboratory for Materials Science, Institute of Metal Research, Chinese Academy of Sciences 72 Wenhua RD, Shenyang 110016, China.
† These authors contributed equally to the research.
Electronic Supplementary Information (ESI) available: [Microscopic observation and XRD of microcrystals and UV-vis optical absorption diffuse reflectance curves]. See DOI: 10.1039/x0xx00000x

understand PEC performance of each crystal facet, microcrystals/2 dimensional (2D) thin film of photocatalysts with selectively exposed crystal facet would be required. However, directly grown TiO_2 thin film with selectively exposed dominant crystal facet from substrate has not been reported with hydrothermal/solvothermal methods.[20,21] It is difficult to prepare photocatalyst microcrystal thin films which could expose single facet selectively and even more, suitable methodology is very rare to prove real PEC performance of the selected single crystal facet. Single crystal facet exposed thin films have been usually fabricated by deposition such as chemical vapor deposition and atomic layer deposition.[22] However, these deposition techniques are typically expensive, slow, providing a limited choice of active materials and not available for the large surface area.[23] In addition, they cannot modulate the facet selectivity of the photocatalysts and it could not be expected to improve PEC performance from facet engineering.

In the present study, we demonstrate selectively exposed crystal facet-engineered TiO_2 thin film photoanode. Based on our previous research about synthesis of microcrystals[24] and second-hydrothermal reaction,[20,25,26] we suggest the methodology for metal oxide photoanode with selectively exposed crystal facet. Selectively exposed crystal faceted TiO_2 thin film photoanode has been comparatively studied for practical PEC performance such as hydrogen evolution between TiO_2 photoanode with selectively exposed each (101), (100), and (001) crystal facet. This suggested methodology first demonstrates scientific significance on their PEC performance depending on selectively exposed crystal facet of TiO_2 thin film. We hope that the results of this study contribute to design the efficient metal oxide photoanode for the enhanced solar fuel production.

Experimental

Materials.

Titanium oxysulfate-sulfuric acid complex hydrate ($TiOSO_4 \bullet xH_2SO_4 \bullet xH_2O$, FW:276 g mol^{-1}, Sigma-Aldrich, synthesis grade), titanium (powder, -100 mesh, 99.7% metal basis), hydrogen fluoride (48~50% of HF, J.T.Baker), polyethyleneimine (PEI) and ethyl alcohol were used without any further purifications. Distilled water was used with milli-Q gradient included Quantum EX Cartridge Filter from EMD Millipore. F-doped tin oxide (FTO) coated glass (2 cm x 2 cm) obtained from Pilkington (Toledo, OH) was employed as a transparent conducting oxide.

Synthesis of dominantly (101) facet exposed TiO_2 microcrystals (TO_{101}).

TO_{101} bi-pyramidal microcrystals were synthesized by adding Ti powder (0.006 g), hydrogen peroxide (3 mL), HF (0.064 mL, 48~50%, 53 mM) and D.W. (27 mL) into a microwave reaction vessel. The prepared mixture was continuously stirred for 3 hrs until a clear yellow solution was obtained. The microwave hydrothermal treatment was carried out in a MARS (0-1200 watts ± 15%, 2450 MHz, CEM Corporation). The temperature and pressure were controlled with a RTP-300 Plus and ESP-1500 Plus sensor, respectively. The reaction was performed at 180 °C for 4 hrs. After the reaction was completed, the reactor was cooled with flowing water and the white powder product was collected by centrifugation, washed several times and was dried. For the synthesis of dominantly (100) facet exposed TiO_2 (TO_{100}, rectangular-shape) and dominantly (001) facet exposed TiO_2 (TO_{001}, plate-shape) microcrystal, each 45 mM and 85 mM aqueous HF solution was used into reaction. Titanium oxysulfate-sulfuric acid complex hydrate (100 mg) was dissolved in each prepared 45 mM and 85 mM aqueous HF solution (133 mL) and stirred for 2 hrs until the suspensions became transparent. The resultant solutions were transferred to Teflon lined autoclaves and heated at 180 ℃ for 2 hrs (TO_{100}) and 12 hrs (TO_{001}), respectively. After the reaction was complete, the same procedure was applied as described above. The as-prepared white resultants (TO_{101}, TO_{100} and TO_{001}) were heated at 600 °C under air in a furnace for 2 hrs.

Fabrication of secondary reacted thin film photoanodes (sTO_{101}, sTO_{100} and sTO_{001}).

A clean FTO was spin-coated with 2.0 wt % PEI at a speed at 2000 rpm for 20 s. The as-synthesized TiO_2 microcrystals (TO_{101}, TO_{100} and TO_{001}) were placed and assembled on the PEI-coated substrates. As-prepared monolayer film (mTO_{101}, mTO_{100} and mTO_{001}) was heat-treated at 500 °C for 3 hrs to remove the polymeric linker of PEI. For a typical synthesis of sTO_{100}, mTO_{100} was placed in a similar solution as previously used to prepare TO_{100} for 2 hrs. mTO_{100} was then transferred to an oven and heated at 200 ℃ for 2 hrs. mTO_{101} and mTO_{001} were placed in a solution containing 35 wt% HCl (0.018 mL), TiF_4 (0.10 g), NaCl (0.935 g) and D.W. (20 mL) and secondly reacted at 200 °C for 1.5 hrs and 4 hrs, respectively, for sTO_{101} and sTO_{001} photoanodes. Each of the secondary grown TiO_2 films (sTO_{101}, sTO_{100}, sTO_{001}) was annealed at 500 °C for 3 hrs.

Characterization.

The crystallographic information for all the samples was obtained by X-ray diffraction (XRD) (Rigaku miniFlex-II desktop X-ray diffractometer, Cu Kα radiation with λ = 0.154056 nm). The microscopic observation of all the samples was carried out with field emission scanning electron microscopy (Hitachi S-4300 FE-SEM). Transmission electron microscope (TEM) image and selected area (electron) diffraction (SAED) pattern were obtained with a JEOL transmission electron microscope (JEM 2100F) at 200 keV accelerating voltage. The optical properties including band energies of all the samples were monitored and determined from diffuse reflectance spectra (DRS) by Varian Cary 5000 UV-Vis-NIR Spectrophotometer (Agilent Technologies) and FTO glass was used as the reference to characterize the absorbance.

Photoelectrochemical measurements.

Photoelectrochemical measurements of photoanodes as working electrode were conducted with a PL-9 potentiostat as a conventional three-electrode system. A 300 W Xe arc lamp

was used for the simulated solar illumination through an AM 1.5 G filter (Asahi HAL-320, 100 mW cm^{-2}). Before PEC measurement, the power density of the incident light was adjusted to 100 mW cm^{-2} using a NREL certified reference cell (Photo Emission Tech., Inc.). The illumination was set as a back-side illumination to FTO surface. The illuminated area was 0.38 cm^2 of a circle (0.7 cm of diameter) at room temperature under 1 sun illumination. With employing Pt electrode and Ag/AgCl reference electrode in aqueous Na_2SO_4 solution (0.5 M, pH = 6.8), I-V curve was plotted at a scan rate of 20 mV s^{-1} with scanning the potential to the positive direction. I-t curve was observed under constant bias. All the PEC measurement was set using Ag/AgCl (2.0 M of KCl) reference electrode. Electrochemical impedance spectroscopy (EIS) curves were obtained from 0.1 to 105 Hz and recorded at 0.65 V vs. Ag/AgCl. Incident photon to current conversion efficiency (IPCE) was determined from 300 to 800 nm with an applied potential of 0.65 V.

Hydrogen gas production measurements.

Hydrogen gas evolution experiments were carried out in air-tight continuous flow cell connecting with the online GC system (Agilent 7890A) equipped with pulsed discharged detector (PDD). A 30 mL of PEC cell consisted of nafion 117 proton transfer material between the photoanode and Pt counter electrode, respectively. 1.13 cm^2 of illuminated area in photoanode and Pt counter electrode was applied into separately 15 mL of 0.5 M Na_2SO_4 aqueous solution with Ag/AgCl as a reference electrode. After He gas (99.9999 %) flushed at the flow rate 10 mL min^{-1} for 3 hrs to remove the air under dark condition, working electrode was illuminated at the continuous flow of He (10 mL min^{-1}). The evolved gas was checked every hour for 12 hrs at 0.65 V (vs Ag/AgCl) with 1500 rpm of stirring at room temperature under 1 sun irradiation (Asahi HAL-320, 100 mW cm^{-2}). The complete water splitting reaction require total potential 1.23 eV (RHE) which is equivalent to 0.65 V (vs Ag/AgCl) (Supporting Information).

Electrical conductivity measurements.

Electrical conductivity measurements depending facets in TiO_2 microcrystals were carried out by obtaining I-V curves with a probe station, which was installed in Shenyang Nation Laboratory for Materials Science (Prof. H-M. Cheng, Institute of Metal Research, China). A one drop of TiO_2 microcrystals in ethanol was placed on a silicon substrate and dried. The substrate was loaded into a field emission scanning electron microscope (FE-SEM, NOVA NANOSEM 430) with two pico-probe tungsten tips (PT-14-6705-13), which were set into the arms with a Kleindieknanotechnik controller. For measuring the I-V curves, a Keithly semiconductor characterization system (4200-SCS) was connected to the two tungsten tips. The current was checked with a potential range of -0.5 to 5.0 V.

Experimental details for fluorescence lifetime measurements.

Fluorescence lifetime decays were measured using an inverted-type scanning confocal microscope (MicroTime-200, Picoquant, Germany) with a 20x objective. The measurements were performed at the Korea Basic Science Institute (KBSI), Daegu Center, South Korea. A single-mode pulsed diode laser (375 nm with an instrumental response function of ~240 ps in pulse width, a repetition rate of 5 MHz, and a laser power of ~5 μW) was used as an excitation source. A dichroic mirror (Z375RDC, AHF), a longpass filter (HQ405lp, AHF), and an avalanche photodiode detector (PDM series, MPD) was used to collect entire emission from the film samples. Time-resolved fluorescence photon counting and exponential fitting for the obtained fluorescence decays were performed using the Symphotime software (version 5.3).

Results and discussion

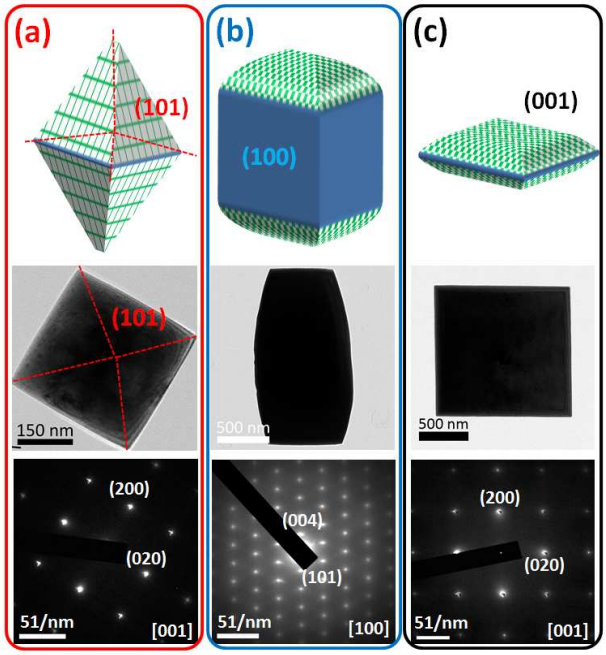

Fig. 1 Scheme, typical TEM images and SAED pattern of bi-pyramidal TO_{101} (a), cuboid TO_{100} (b) and plate TO_{001} (c) microcrystals.

For 100% selectively exposed-(101) facet in TiO_2 microcrystal (TO_{101}), bi-pyramidal TiO_2 microcrystal, was newly designed and prepared with H_2O_2 and HF. For comparison of crystal facet-dependent photochemical properties, TiO_2 microcrystals with dominantly exposed (100) and (001) facets (TO_{100} and TO_{001}) were synthesized by controlling the atomic ratio of Ti/F in the precursor solutions.[27] Microscopic observation of each TiO_2 microcrystal was determined in high resolution transmission electron microscopy (HRTEM) and selected area electron diffraction (SAED) of Figure 1. TO_{101} was determined as bi-pyramidal shaped microcrystal with 300 nm x 300 nm dimension. With scanning electron microscopic (SEM) image in Figure S1 (Supporting Information), it indicated that all exposed facet was 8-(101) facets. TO_{100} was cuboid-shaped microcrystal with 1.1 μm x 1.5 μm dimension. It revealed up/downward 2-(001) facets surrounding lateral 4-(100)

facets. TO_{001} shows plate-shaped microcrystal with 1.5 μm x 1.5 μm dimension, exposing dominantly up/downward 2-(001) facets. Their microscopic observation in Figure 1 and S2 with matched with crystallographic information of X-ray powder diffraction (XRD) in Figure S3. It indicates that the lattice fringe of TO_{101}, TO_{100}, TO_{001} with d spacing values of 0.133, 0.237, and 0.189 nm corresponds to (220), (004), and (200) facets, respectively. All the samples, TO_{101}, TO_{100}, TO_{001} are determined to be single crystalline microcrystals and each TiO_2 microcrystal appears to be dominantly exposed with selected (101), (100) and (001) crystal facet, respectively.

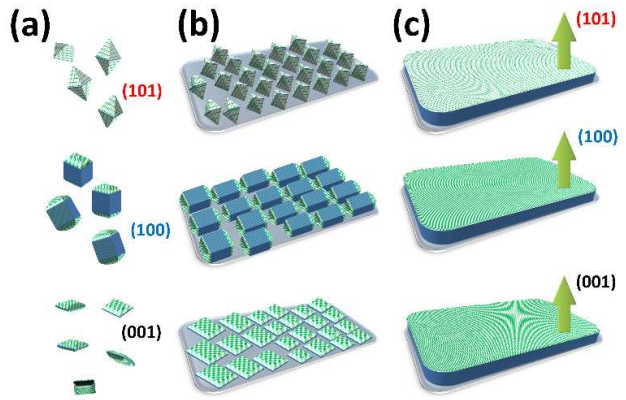

Fig. 2 Scheme of upward-facet exposed metal oxide photoanode. Metal oxide microcrystals (a) was assembled to monolayer-film (b) and upward-faceted film (c) was fabricated via second-hydrothermal reaction.

Each TO microcrystal with each dominantly exposed crystal facet was introduced for a one-axis oriented TiO_2 monolayer (mTO) photoanode to study the facet dependent PEC performance. A one-axis oriented monolayer of each TO microcrystal was fabricated by polyethyleneimine (PEI)-induced manual assembly technique, which can be used to prepare 2D monolayer with each exposed crystal facet.[24-26] Selectively exposed crystal facet-manipulated TiO_2 thin film photoanode is fabricated through a three-step strategy in Figure 2. Pre-synthesized TiO_2 microcrystal with each dominant crystal facet was positioned on the FTO with PEI-induced manual assembly, in which the imine group of PEI formed a covalent bond with oxygen on the FTO surface.[28,29] It resulted in the formation of the monolayer of TiO_2 microcrystals on the substrate surface. Each TO microcrystal is aligned and its dominantly exposed facet is upward. After that, secondary growth hydrothermal reaction drives upward-growth from substrate. Voids among TiO_2 microcrystals were filled and the rest facets were covered and finally resulted in TiO_2 thin films with selective upward-targeted crystal facet exposure. As shown in Figure 2, by PEI-induced manual assembly on FTO glass, each TO microcrystal was assembled to form a monolayer thin film. Figure 2 (b) shows schematic illustrations of monolayered TO_{101} film (mTO_{101}), monolayered TO_{100} film (mTO_{100}) and monolayered TO_{001} film (mTO_{001}) after PEI-induced manual assembly. Figure 2 (c) shows schematic illustrations of the secondary grown TO_{101} film (sTO_{101}), TO_{100} film (sTO_{100}) and TO_{001} film (sTO_{001}), respectively.

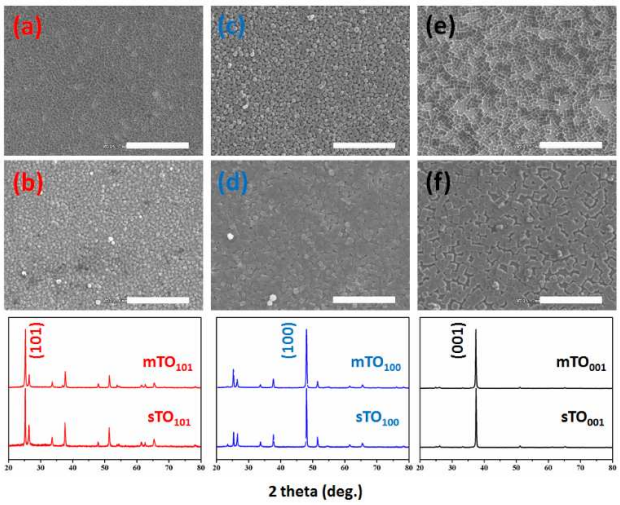

Fig. 3 Typical SEM images and XRD of mTO_{101} (a), sTO_{101} (b), mTO_{100} (c), sTO_{100} (d), mTO_{001} (e) and sTO_{001} (f). (Scale bar in SEM images; 20 μm).

In Figure 3 and S4, typical SEM images shows that the voids and gaps among the microcrystals were filled and lateral facets were covered by the secondary growth hydrothermal reaction. With each exposed crystal facet, c-axis of sTO was matched with the most intensive XRD peak. mTO_{101} with exposed all 7-(101) facets was vertically aligned to [101] as a c-axis. It resulted in the most intensive peak corresponding to (101) at 25° from XRD pattern with the other peaks from FTO substrate. Likewise, 4-(100) and 2-(001) facets exposed mTO_{100} and dominant 2-(001) facets exposed mTO_{001} were vertically aligned to [100] and [001] as a c-axis and resulted in (100) and (001) at 48° and 37.5°, respectively, from XRD spectra. Interestingly, after the other crystal facets in mTO were covered from the secondary grown hydrothermal reaction, upward facet of mTO such as (101) in mTO_{101}, (100) in mTO_{100} and (001) in mTO_{001} stayed as upward exposure. SEM and XRD of sTO clearly indicate that (101) facet in sTO_{101}, (100) facet in sTO_{100} and (001) facet in sTO_{001} stayed as upward exposure facets and their perpendicular orientation was also remained as c-axis in Figure 4.

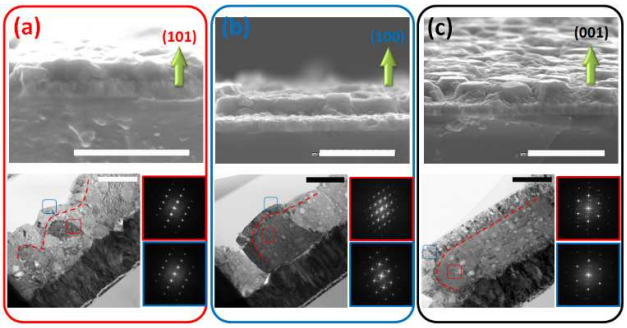

Fig. 4 Typical cross-sectional SEM (Scale bar; 5 μm), TEM images (Scale bar; 0.2 μm) and FFT images (red square; former crystal, blue square; latter crystal) of sTO_{101} (a), sTO_{100} (b) and sTO_{001} (c).

Apparently, cross-sectional TEM images by focused ion beam (FIB) provided that upward crystal facet in each sTO was grown along c-axis as a growth direction after secondary grown hydrothermal reaction. It is worthy noted that the crystal phase formed by the secondary growth was distinguishable from the pre-existing single crystal phase (mTO) and it was single crystalline with the same growth direction as shown in cross sectional TEM images and fast fourier transform (FFT) images. SEM images of the mTO and sTO films in Figure S5 and S6 indicate that film thickness of sTO_{101} was determined as 0.937 μm from 0.781 μm of mTO_{101}. The thicknesses of sTO_{100} (0.984 μm) and sTO_{001} (1.015 μm) were also increased from mTO_{100} (0.765 μm) and mTO_{001} (0.796 μm). Based on its approach, our microscopic and crystallographic observations supported that TiO_2 thin film photoanode with exclusively exposed crystal facet on the FTO substrate was successfully fabricated.

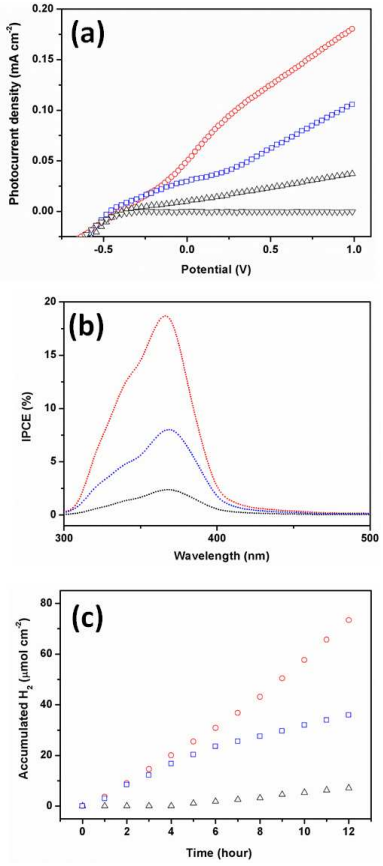

Fig. 5 I-V curve (a), IPCE (b) and gas evolution rate (c) of sTO_{101} (red), sTO_{100} (blue) and sTO_{001} (black).

PEI-induced manual assembly technique arranges one selective crystal facet-exposed TiO_2 particle monolayer films spontaneously on the substrate for making one-axis oriented monolayer. In addition, it also allows comparative study on the real efficiency of one-axis oriented TiO_2 thin films with selectively exposed single crystal facet in the actual PEC system. Figure 5 show that photocurrent density of sTO_{101}, sTO_{100} and sTO_{001} at 0.65 V were determined to be 0.13, 0.07, and 0.02 mA cm^{-2}, respectively. Even all TiO_2 thin film photoanodes show -0.5 V (vs Ag/AgCl) of onset potential (V_{op}), such tendency of photocurrent density from each facet was matched with the order of the incident photon to electron conversion efficiency (IPCE) values of each TiO_2 thin film photoanode. All sTO revealed 367 nm of λ_{max} and 460 nm of onset wavelength (λ_{op}). A sTO_{101} produced the highest IPCE value as 18%, which was compared with 8% of sTO100 and 2% of sTO_{001} at 367 nm of λ_{max}. The hydrogen evolution efficiency was also investigated for sTO_{101}, sTO_{100}, and sTO_{001} based on the facet dependent I-V and IPCE results. Under hydrogen gas evolution condition in Figure S7, Figure 5 (c) and S8 shows hydrogen gas evolution rate for the sTO photoanode under AM 1.5 G. It is worthy noted that sTO_{101} showed the largest amount of hydrogen gas evolution as 73 μmol cm^{-2} compared with 36 μmol cm^{-2} of sTO_{100} and 7 μmol cm^{-2} of sTO_{001}, respectively, for 12 hrs. Under UV irradiation, hydrogen gas evolution of sTO_{101} reached to 1.0 mmol cm^{-2} and sTO_{100} and sTO_{001} produced 0.8 mmol cm^{-2} and 0.3 mmol cm^{-2}, respectively, as shown in Figure S9. The solar-to-hydrogen conversion efficiency ($_{\eta}$STH) was measured in a 3-eletrode system using following equation, assuming faradaic efficiency as 100% when considering applied potential.[30] $_{\eta}$STH is beneficial in describing the whole compartments of PEC for water splitting. Interestingly, the $_{\eta}$STH of sTO_{101} was calculated to be 0.077% at 0.65 V. This enhancement on $_{\eta}$STH in sTO_{101} come from along (101)-axis, in which the crystal facet dependent PEC performance was comparable with 0.053% in the previous report.[30] Typical $_{\eta}$STH values of sTO_{100} and sTO_{001} were determined as 0.040% and 0.012% , respectively.

Strikingly, these results are not consistent with the study predicted by computational calculation on the surface energy of each facet of TiO_2 microcrystal. Theoretically PEC performance has been demonstrated as an ordering (001) > (100) > (101) facet based on their surface energy of the anatase TiO_2 microcrystal.[31] Although dominant exposure of crystal facet in TiO_2 microcrystals was compared and surface energy of the (001) facet is thermodynamically the highest one, our observation apparently indicated that sTO_{101} produced coherently the highest PEC performance. For better understanding of PEC ordering as sTO_{101} > sTO_{100} > sTO_{001}, each TiO_2 thin film photoanode was studied in aspect of light harvesting, electrical conductivity and interfacial impedance. The light harvesting ability of the each TiO_2 thin film photoanode was investigated by determining their optical absorption coefficient in Figure S10. Optical absorption coefficient was decreased from 16.7 nm^{-1} of sTO_{101} to 13.4 nm^{-1} and 16.6 nm^{-1} of sTO_{100} and sTO_{001}, respectively. Additionally, the electrical conductivity was investigated with the facet of TO microcrystals by contacting the selected crystal facets with a probe station with tungsten tips.[32] Images of the surface current measurements using probe station are shown in the inset of Figure 6. The electrical conductivity along the c-axis of the TO microcrystals with different crystal facets was determined between -5.0 and 5.0 V. The electrical connection

on between (001) facets in TO_{001} microcrystals produced the surface current as c.a. 10 μA. Even surface current on between (001) and (101) facets in TO_{001} microcrystals showed as c.a. 30 μA. The highest current was observed as ca. 50 μA in the electrical connection on between (101) facets. The results show that electrical conductivity caused by electrical connection on two (101) facets of TO microcrystal was the highest. Electrical connection is more favorable between (101) facets than others.

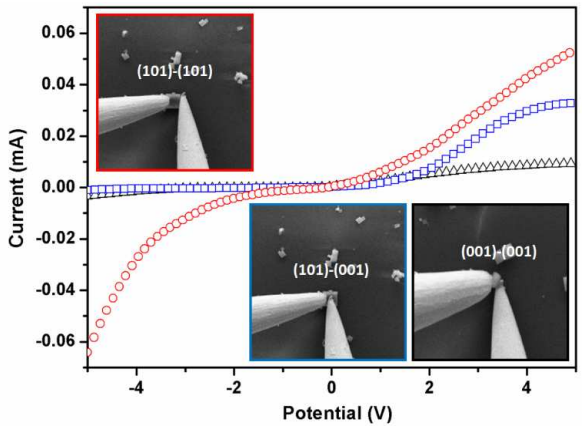

Fig. 6 Facet-depending electrical conductivity between (101) and (101) in sTO_{101} (red), (101) and (001) (blue), and (001)-(001) in sTO_{001} (black).

Together with facet dependent-optical and electrical properties, interfacial impedance between the surface of TiO_2 thin film with each crystal facet and electrolyte solution was measured for interfacial charge transfer through the interface in Figure 7, which shows the comparison of Nyquist plots among the sTO photoanodes. The electrical impedance spectroscopy (EIS) experiments determine the charge transfer resistance (R_{ct}) at the interface between surface of TiO_2 thin film photoanodes with each crystal facet and the electrolyte solution under solar light illumination. In the Nyquist plots of sTO thin film photoanodes, the presence of semicircles is related to the charge-transfer resistance at the counter electrode, electron transport at the interface of photoelectrode/electrolyte solution and the mass transport in electrolyte.[33] Especially, the secondary arc of the Nyquist plots is attributed to the interfacial charge transfer kinetics. Since the semicircle is derived from the recombination resistance at the interface between the surface of TiO_2 thin film photoanode with each crystal facet and electrolyte solution, the resistance value increases in the following order: sTO_{101} < sTO_{100} < sTO_{001}. Among them, sTO_{101} exhibits the highest photovoltaic performance, owing to its low interfacial impedance for charge transfer.[33] This enhanced PEC performance for the kinetics of photogenerated charge carriers was confirmed with time-resolved photoluminescence (TRPL) at room temperature in Figure 7 (b). From the excitation wavelength at 375 nm, transient emission was observed in sTO_{101} (red), sTO_{100} (blue) and sTO_{001} (black), respectively. The average decay time (τ_{ave}) of the charge carriers in sTO_{101} was 20.832 ns which is longest τ_{ave} compared with 11.319 ns and 10.337 ns in sTO_{100} and sTO_{001}, respectively. τ_{ave} of the charge carriers in sTO_{101} is significantly increased compared with those in sTO_{100} and sTO_{001}, which indicates that the (101)-crystal facet in sTO_{101} enhances the charge separation efficiency and retards charge recombination at the interfacial solid-liquid junction.

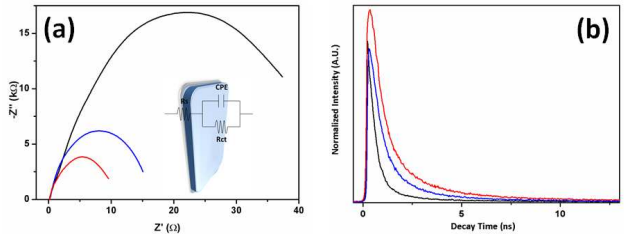

Fig. 7 Nyquist plot (a) and time resolved photoluminescence (b) in sTO_{101} (red), sTO_{100} (blue) and sTO_{001} (black).

The impedance at the interface between TiO_2 thin film photoanode and electrolyte solution was the lowest for sTO_{101}. The order of interface impedance values of the sTO reveals that the higher photoreactive properties of sTO_{101} are related to its higher faradaic current. In addition, the diffusivity of photo-generated electrons in the TiO_2 thin film photoanode could be proved with the electron mobility along c-axis, like (101), (100), and (001) axis, because electrons transport along the c-axis of TiO_2 thin film photoanodes and reaches the transparent conducting substrate to determine the photocurrent density of the considering photoanode. Electron diffusion along c-axis of the TiO_2 thin film photoanode can be controlled by the bond lengths between Ti and O in the three-dimensional crystal structure of the regular repeating layers of TiO_2.[34] The three dimensional crystal structures of anatase TiO_2 microcrystal along the (101), (100), and (001) facets are shown in Figure 8. A short bond length of the regular atomic arrangement in the crystal structures of TiO_2 particles allows faster electron diffusivity along the c-axis. In Figure 8, the distance between layers along the (101)-axis was the shortest (0.371 nm). Thus, electrons can be diffused along the (101)-axis faster than the other axes. The lengths between layers along the (100) and (001)-axis were calculated as 0.379 and 0.506 nm, respectively. In addition to electrical conductivity, interfacial resistance and diffusivity of charge along the c-axis are also critical parameters for the PEC performance of each crystal facet. An extraordinary high PEC performance of TiO_2 thin film photoanode with (101) facet was attributed to the electrical conductivity, interfacial resistance and diffusivity of charge along the c-axis.

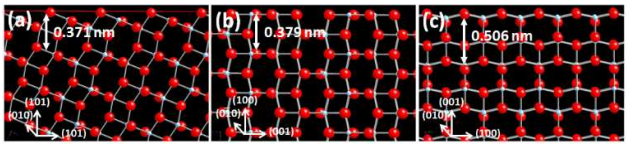

Fig. 8 Three-dimensional atomic arrangement structure of anatase TiO_2 microcrystals along the (101), (100), and (001) facet. The surface crystal structure of facet controlled TiO_2 was simulated by crystal maker™ software based on the structure of anatase TiO_2 (a = 3.785, b = 3.785, c = 9.5140, α = β = γ = 90°).

Conclusions

In summary, we demonstrated that TiO_2 thin film photoanode with selectively exposed crystal facet was better for higher performance of efficient hydrogen gas evolution. Each facet-exposed TiO_2 thin film photoanode was fabricated using TiO_2 microcrystals with exclusively dominant exposure of each (101), (100), and (001) facet by PEI induced manual assembly technique and the secondary growth hydrothermal reaction. Fabrication of selectively exposed each (101), (100), and (001) crystal facet of TiO_2 thin film photoanode, which have different c-axis arrangements, was carried out to study comparative PEC performance of each crystal facet of TiO_2 thin film photoanode. We observed the higher PEC performance of TiO_2 thin film photoanode with selectively exposed (101) crystal facet than those of (100) and (001) facet. We approached the reason that selectively exposed (101) crystal facet produced favorably higher improvement in the aspect of the electrical conductivity, interfacial resistance and diffusivity of charge along the c-axis. Along with the photocurrent density trend, similar trends in optical absorption coefficient, electron diffusivity, IPCE, energy barrier at the interface of TiO_2 thin film photoanode/electrolyte solution supported the water splitting reaction efficiency of each different crystal facet of TiO_2 thin film photoanode. sTO_{101} showed the largest amount of hydrogen gas evolution, which could be attributed to the largest photon absorption capacity on the (101) crystal surface, highest electron diffusivity along c-axis, highest IPCE, and lowest resistance at the interface of sTO_{101}/electrolyte solution.

Acknowledgements

Artificial Photosynthesis (KCAP) located in Sogang University (No.2009-0093885) funded by the Minister of Science, ICT and Future Planning (MSIP) through the National Research Foundation of Korea and the Brain Korea 21 Plus Project 2015. The authors thank Dr. Weon-Sik Chae, KBSI Daegu Center, for the fluorescence lifetime measurements.

Notes and references

1 D. Kim, K. K. Sakimoto, D. Hong and P. Yang, *Angew. Chem. Int. Ed.* 2015, **54**, 3259-3266.
2 M. G. Walter, E. L. Warren, J. R. McKone, S. W. Boettcher, Q. Mi, E. A. Santori and N. S. Lewis, *Chem. Rev.* 2010, **110**, 6446-6473.
3 Y. Ma, X. Wang, Y. Jia, X. Chen, H. Han and C. Li, *Chem. Rev.* 2014, **114**, 9987-10043.
4 Y. Tachibana, N. Vayssieres and J. R. Durrant, *Nat. Photonics.* 2012, **6**, 511-518.
5 J. Barber, *Chem. Soc. Rev.* 2009, **38**, 185-196.
6 N. S. Lewis and D. G. Nocera, *Proc. Natl Acad. Sci. USA* 2006, **103**, 15729-15735.
7 Z. Chen, H. Dinh and E. Miller, Photoelectrochemical Water Splitting: Standards, Experimental Methods, and Protocols. Springer. 2013.
8 G. Liu, H. G. Yang, J. Pan, Y. Q. Yang, G. Q. (Max) Lu and H-M. Cheng, *Chem. Rev.* 2014, **114**, 9559-9612.
9 J. Pan, G. Liu, G. Q. (Max) Lu and H-M. Cheng, *Angew. Chem. Int. Ed.* 2011, **50**, 2133-2137.
10 F-R. Fan, Y. Ding, D-Y. Liu, Z-Q. Tian and Z. L. Wang, *J. Am. Chem. Soc.* 2009, **131**, 12036-12037.
11 J. Joo, B. Y. Chow, M. Prakash and E. S. Boyden, *Nat. Mater.* 2011, **10**, 596-601.
12 Y. P. Xie, G. Liu, L. Yin and H-M. Cheng, *J. Mater. Chem.* 2012, **22**, 6746-6751.
13 S. Sun, X. Song, Y. Sun, D. Deng and Z. Yang, *Catal. Sci. Technol.* 2012, **2**, 925-930.
14 D. Wang, H. Jiang, X. Zong, Q. Xu, Y. Ma, G. Li and C. Li, *Chem. Eur. J.* 2011, **17**, 1275-1282.
15 D-H. Wang, G-Q. Gao, Y-W. Zhang, L-S. Zhou, A-W. Xu and W. Chen, *Nanoscale,* 2012, **4**, 7780-7785.
16 H. Cheng, B. Huang and Y. Dai, *Nanoscale,* 2014, **6**, 2009-2026.
17 W-N. Zhao and Z-P. Liu, *Chem. Sci.* 2014, **5**, 2256-2264.
18 J. Yang, D. Wang, X. Zhuo and C. Li, *Chem. Eur. J.* 2013, **19**, 1320-1326.
19 H. G. Yang, C. H. Sun, S. Z. Qiao, J. Zou, G. Liu, S. C. Smith, H-M. Cheng and G. Q. Lu, *Nature* 2008, **453**, 638-641.
20 T. K. Van, C. K. Nguyen and Y. S. Kang, *Chem. Eur. J.* 2013, **19**, 9376-9380.
21 B. Liu and E. S. Aydil, *Chem. Commun.* 2011, **47**, 9507-9509.
22 D. A. Boyd, L. Greengard, M. Brongersma, M. Y. El-Naggar and D. G. Goodwin, *Nano Lett.* 2006, **6**, 2592-2597.
23 J. Liu, H. G. Zhang, J. Wang, J. Cho, J. H. Pikul, E. S. Epstein, X. Huang, J. Liu, W. P. King and P. V. Braun, *Adv. Mater.* 2014, **26**, 7096-7101.
24 C. W. Kim, Y. S. Son, A. U. Pawar, M. J. Kang, J. Y. Zheng, V. Sharma, P. Mohanty and Y. S. Kang, *J. Mater. Chem. A.* 2014, **2**, 6057-6066.
25 H. G. Cha, M. J. Kang, I. C. Hwang, H. Kim, K. B. Yoon and Y. S. Kang, *Chem. Commun.* 2015, **51**, 6407-6410.
26 J. Y. Zheng, G. Song, J. Hong, T. K. Van, A. U. Pawar, D. Y. Kim, C. W. Kim, Z. Haider and Y. S. Kang, *Cryst. Growth Des.* 2014, **14**, 19867-19872.
27 L. Pan, J. J. Zou, S. Wang, X. Y. Liu, X. Zheng and L. Wang, *ACS Appl. Mater. Interface* 2012, **4**, 1650-1655.
28 J. S. Lee, Y-J. Lee, E. L. Tae, Y. S. Park and K. B. Yoon, *Science*, 2003, **301**, 818-821.
29 T. C. T. Pham, H. S. Kim and K. B. Yoon, *Angew. Chem. Int. Ed.* 2013, **52**, 5539-5543.
30 E. S. Kim, N. Nishimura, G. Magesh, J. Y. Kim, J. W. Jang, H. Jun, J. Kubota, K. Domen and J. S. Lee, *J. Am. Chem. Soc.* 2013, **135**, 5375-5383.
31 M. Lazzeri, A. Vittadini and A. Selloni, *Phy. Rev. B* 2001, **63**, 155401-155409.
32 C. H. Kuo, Y. C. Yang, S. Gwo and M. H. Huang, *J. Am. Chem. Soc.* 2011, **133**, 1052-1057.
33 E. Barsoukov and J. R. Macdonald, Impedance Spectroscopy. Wiley &Sons, Inc. Hoboken. New Jersey, 2005.
34 P. S. Archana, R. Jose, C. Vijila and S. Ramakrishna, *J. Phys. Chem. C* 2009, **113**, 21538-21542.

Table of Contents Graphic and Synopsis